

# SparseGS-W: Sparse-View 3D Gaussian Splatting in the Wild with Generative Priors

Yiqing Li<sup>1</sup>, Xuan Wang<sup>2</sup>, Jiawei Wu<sup>1</sup>, Yikun Ma<sup>1</sup>, Zhi Jin<sup>1\*</sup>  
<sup>1</sup>Sun Yat-sen University <sup>2</sup>Ant Research

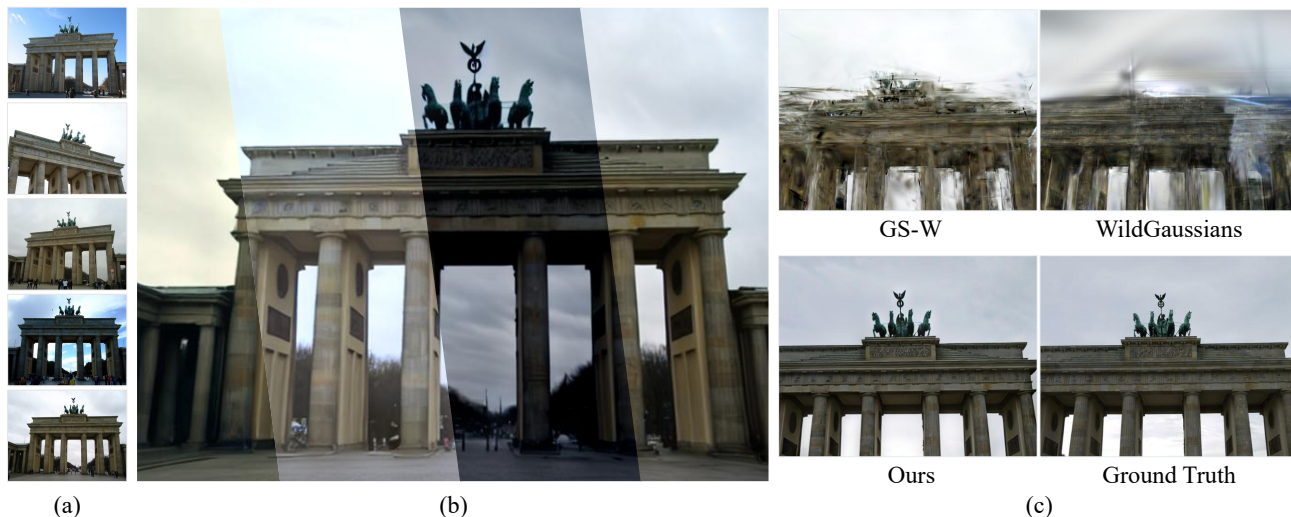


Figure 1. Given only 5 tourism images captured from different views and times, either from a user’s photo album or the Internet (a), our method is able to reconstruct the landscape with variable appearances and remove transient occlusions (b). Our method outperforms previous state-of-the-art methods GS-W [49] and WildGaussians [17] (c).

## Abstract

Synthesizing novel views of large-scale scenes from unconstrained in-the-wild images is an important but challenging task in computer vision. Existing methods, which optimize per-image appearance and transient occlusion through implicit neural networks from dense training views (approximately 1000 images), struggle to perform effectively under sparse input conditions, resulting in noticeable artifacts. To this end, we propose SparseGS-W, a novel framework based on 3D Gaussian Splatting that enables the reconstruction of complex outdoor scenes and handles occlusions and appearance changes with as few as five training images. We leverage geometric priors and constrained diffusion priors to compensate for the lack of multi-view information from extremely sparse input. Specifically, we propose a plug-and-play Constrained Novel-View Enhancement module to iteratively improve the quality of rendered novel views during the Gaussian optimization process. Furthermore, we propose an Occlusion Handling module, which flexibly re-

moves occlusions utilizing the inherent high-quality inpainting capability of constrained diffusion priors. Both modules are capable of extracting appearance features from any user-provided reference image, enabling flexible modeling of illumination-consistent scenes. Extensive experiments on the PhotoTourism and Tanks and Temples datasets demonstrate that SparseGS-W achieves state-of-the-art performance not only in full-reference metrics, but also in commonly used non-reference metrics such as FID, ClipIQ, and MUSIQ.

## 1. Introduction

Novel view synthesis (NVS) from unconstrained photo collections is a long-standing challenge in the field of computer vision, with significant importance in areas such as virtual reality and augmented reality. Neural Radiance Field (NeRF) [23] has made remarkable progress by significantly improving the quality and consistency of images rendered from arbitrary views. Recently, 3D Gaussian Splatting (3DGS) [15] has introduced an explicit point-based repre-

\*Corresponding author

sensation, achieving high-quality and real-time rendering. However, both methods are designed to model static scenes, lacking mechanisms for handling real-world datasets, such as large-scale Internet photo collections of tourist landmarks. These datasets usually consist of images captured at various times, from different viewpoints, under variable illumination, and often contain occlusions.

To address the aforementioned problems, previous NeRF-based and 3DGS-based methods [2, 3, 17, 22, 40, 44, 46, 49] incorporate neural networks to extract per-image appearance features and transient occlusions. However, above methods fundamentally rely on neural networks by leveraging the spatial consistency of static objects across densely captured views (approximately 1000 images), which makes it challenging to achieve high-quality rendering in extremely few-shot settings. As shown in Fig. 1(c), previous methods [17, 49] produce noticeable elongated artifacts with only 5 input views.

The primary challenge lies in the coupling of multiple difficulties, including sparse inputs, transient occlusions, and dynamic appearance changes. In this work, we propose **SparseGS-W**, a novel framework to achieve high-quality and view-consistent scene reconstruction for sparse unconstrained image collections.

Specifically, we first incorporate a pre-trained multi-view stereo model to obtain camera parameters and dense initial point cloud with rich geometric priors. To provide sufficient and reliable multi-view guidance for 3D Gaussians, we propose a plug-and-play *Constrained Novel-View Enhancement* (CNVE) module, which utilizes constrained diffusion priors and attention injection strategy. The key insight of this module is to reformulate the problem of high-quality and view-consistent novel view synthesis as an iterative image enhancement task. Then, the enhanced views are iteratively exploited as the pseudo supervision for optimizing the 3D Gaussians. We propose an *Occlusion Handling* (OH) module, which leverages the inherent high-quality inpainting capability of the constrained diffusion model to flexibly remove transient occlusions based on the user’s preference. Both modules incorporate a simple yet effective AdaIn [10] operation to flexibly extract appearance features from a given reference image, enabling efficient scene modeling without the need for an additional appearance extraction network. Additionally, we introduce a *Progressive Sampling and Training Strategy* (PSTS) to improve the reconstruction of detail appearance in the scene.

Extensive validations on large-scale PhotoTourism datasets and Tanks and Temples datasets demonstrate that our method achieves state-of-the-art rendering quality and exhibits robust occlusion handling capabilities. Our contributions can be summarized as follows:

- To the best of our knowledge, SparseGS-W is the first framework to handle few-shot novel view synthesis for

unconstrained image collections.

- We propose a plug-and-play *Constrained Novel-View Enhancement* module and an *Occlusion Handling* module, both of which effectively leverage constrained diffusion priors for generating high-quality and view-consistent images free of transient occlusions.
- A *Progressive Sampling and Training Strategy* to control the augmentation and sampling of novel views, as well as the training process of the Gaussian radiation field.

## 2. Related Work

### 2.1. Novel View Synthesis with Sparse Views

NeRF [23] and 3DGS [15], as currently the most used novel view synthesis techniques, require a large number of training images to achieve good performance, which limits their practical applications. To address this, previous NeRFs [4, 16, 25, 34, 45, 47] introduce various regularizations to improve rendering quality with sparse input views. Other methods [4, 11, 31, 37, 43] attempt to introduce additional priors to extend NeRF, enabling similar performance. With the development of 3DGS, some studies [19, 21, 27, 50, 53] have explored using 3DGS as a replacement for NeRF to accomplish the few-shot novel view synthesis task. Notably, FSGS [53] introduces a Gaussian unpooling strategy and incorporates depth priors to guide the optimization of the Gaussian radiance field. CoherentGS [27] and CoR-GS [50] apply different regularization techniques to constrain Gaussian points. DNGaussian [19] further proposes depth regularization and normalization strategy based on depth priors to achieve more precise reconstruction results. However, these methods face challenges when applied to complex in-the-wild image collections, as they assume static scenes and do not consider transient occlusions and variable appearances.

### 2.2. Novel View Synthesis in the Wild

To tackle in-the-wild scenes, NeRF-W [22] optimizes an appearance embedding for each image and trains a Multi-Layer Perceptron (MLP) to model a transient radiance field. Ha-NeRF [2] and CR-NeRF [46] handle transient occlusions by optimizing an image-dependent 2D visibility map. They also introduce CNN-based appearance encoders to predict the global appearance of each image. More recently, GS-W [49] introduces intrinsic and dynamic appearance features to each Gaussian point to model various appearances. WildGaussians [17] extracts appearance embeddings from reference images with a learnable MLP and leverages DINO feature priors [26] to handle occlusions. WildGS [44] introduces an appearance decomposition strategy and an explicit modeling method to handle complex appearance variations. WE-GS [40] designs a lightweight spatial attention module to jointly predict transient masks and ap-

pearance embeddings. However, these methods utilize neural networks to model scenes based on the multi-view consistency of static objects, making it difficult to achieve good performance in the sparse-view setting.

### 2.3. Novel View Synthesis with Generative Priors

Recently, leveraging generative priors for novel view synthesis has proven to be an effective approach. DreamFusion [29] introduces Score Distillation Sampling (SDS) with a pre-trained diffusion model to guide 3D object generation. ProlificDreamer [42] presents variational score distillation, further improving the quality of 3D objects and effectively addressing issues in SDS, such as over-smoothing and over-saturation. Some methods [6, 20, 30] achieve zero-shot NVS by incorporating 3D information into the diffusion prior. However, these methods require extensive training resources and struggle with real-world scenes. 3DGS-Enhancer [21] fine-tunes a video diffusion model and designs a spatial-temporal decoder to achieve consistent NVS for unbounded outdoor scenes. However, it assumes scenes without occlusion or illumination variations and requires several days of training time, which limits its practical applicability to in-the-wild scenarios.

## 3. Preliminary

### 3.1. 3D Gaussian Splatting

3D Gaussian Splatting [15] is a point-based method for explicitly representing 3D scenes. Each Gaussian has learnable attributes: center position  $\boldsymbol{\mu} \in \mathbb{R}^3$ , 3D covariance matrix  $\boldsymbol{\Sigma} \in \mathbb{R}^{3 \times 3}$ , opacity  $o \in \mathbb{R}$  and color  $c$  represented by spherical harmonics. The influence of a 3D Gaussian on a point  $\boldsymbol{x}$  in the 3D world can be written as:

$$G(\boldsymbol{x}) = \frac{1}{(2\pi)^{3/2} |\boldsymbol{\Sigma}|^{1/2}} e^{-\frac{1}{2}(\boldsymbol{x}-\boldsymbol{\mu})^T \boldsymbol{\Sigma}^{-1}(\boldsymbol{x}-\boldsymbol{\mu})}. \quad (1)$$

To facilitate the optimization of the gradient of  $\boldsymbol{\Sigma}$  while preserving its physical properties,  $\boldsymbol{\Sigma}$  is decomposed into two learnable scaling matrix  $\boldsymbol{S}$  and rotation matrix  $\boldsymbol{R}$ . For color rendering, 3D Gaussians are sorted by depth and projected into the 2D image plane, where the color of each pixel is rendered by a rasterizer through alpha-blending.

### 3.2. Diffusion Model

Diffusion Models (DM) [5, 9, 32] are generative models that progressively add random noise to transform a clean image  $\boldsymbol{x}_0 \sim p_{\text{data}}(\boldsymbol{x})$  into Gaussian noise  $\boldsymbol{x}_T \sim \mathcal{N}(\mathbf{0}, \mathbf{I})$  in the forward diffusion process:

$$\boldsymbol{x}_t = \sqrt{\alpha_t} \cdot \boldsymbol{x}_0 + \sqrt{1 - \alpha_t} \cdot \boldsymbol{\epsilon}, \quad \text{where } \boldsymbol{\epsilon} \sim \mathcal{N}(\mathbf{0}, \mathbf{I}). \quad (2)$$

In the reverse diffusion process, a neural network  $\epsilon_\theta(\boldsymbol{x}_t, t)$  is trained to predict the added noise  $\boldsymbol{z}_{t-1}$  and progressively denoise  $\boldsymbol{x}_T$  until a clean image is obtained. This

process can be formulated as:

$$\boldsymbol{z}_{t-1} = \epsilon_\theta(\boldsymbol{x}_t, t). \quad (3)$$

In this work, we leverage the prior knowledge of Stable Diffusion (SD) [32], which is built on a U-Net framework that includes residual blocks, cross-attention blocks, and self-attention blocks. In the self-attention block, the input intermediate features are query ( $\boldsymbol{Q}$ ), key ( $\boldsymbol{K}$ ), and value ( $\boldsymbol{V}$ ). The output feature can be expressed as:

$$\boldsymbol{F} = \text{softmax} \left( \frac{\boldsymbol{Q}\boldsymbol{K}^T}{\sqrt{d}} \right) \boldsymbol{V}, \quad (4)$$

where  $d$  is the dimension of the embedding. Recent studies have shown that the attention mechanism controls spatial layout of the image [24, 36]. We further use the query and key in the self-attention block to preserve the local structure of the image.

## 4. Method

Given a sparse set of unconstrained images, our goal is to reconstruct the view-consistent, occlusion-free scene while allowing for appearance modification based on user’s preference. In Sec. 4.1, we integrate a multi-view stereo model to generate dense 3D points and the corresponding camera poses. In Sec. 4.2, we propose a plug-and-play *Constrained Novel-View Enhancement* module to iteratively enhance the low-quality novel views. To handle transient objects, we propose an *Occlusion Handling* module in Sec. 4.3. A *Progressive Sampling and Training Strategy* is employed to progressively optimize 3D Gaussians in Sec. 4.4. Finally, we describe the optimization process in Sec. 4.5. An overview of our architecture is visualized as Fig. 2.

### 4.1. Dense Initialization

We utilize DUS3R [39], denoted as  $\mathcal{G}_\theta$  to obtain dense 3D points with rich geometric priors and camera parameters. More specifically, given a sparse set of  $N$  images  $\mathcal{I} = \{\boldsymbol{I}_i^{gt}\}_{i=1}^N$ , we can obtain points  $\boldsymbol{P}$  and corresponding camera parameters  $\mathcal{C} = \{\boldsymbol{C}_i\}_{i=1}^N$  as follows:

$$\boldsymbol{P}, \mathcal{C} = \mathcal{G}_\theta(\mathcal{I}). \quad (5)$$

We observe that DUS3R inherently assumes the absence of transient occlusions. This results in the generated points  $\boldsymbol{P}$  containing occlusion textures, which are incorrectly amplified by the diffusion model. To address this, we leverage a pre-trained segmentation model, EVF-SAM [52], to generate corresponding occlusion masks  $\mathcal{M} = \{\boldsymbol{M}_i\}_{i=1}^N$  based on the text prompt by users. We then replace the colors of the occluded regions with Gaussian noise by:

$$\mathcal{I}_{\mathcal{M}} = \{\boldsymbol{M}_i \odot \mathcal{N}(\boldsymbol{\mu}, \boldsymbol{\sigma}^2) + (\mathbf{1} - \boldsymbol{M}_i) \odot \boldsymbol{I}_i^{gt}\}_{i=1}^N, \quad (6)$$

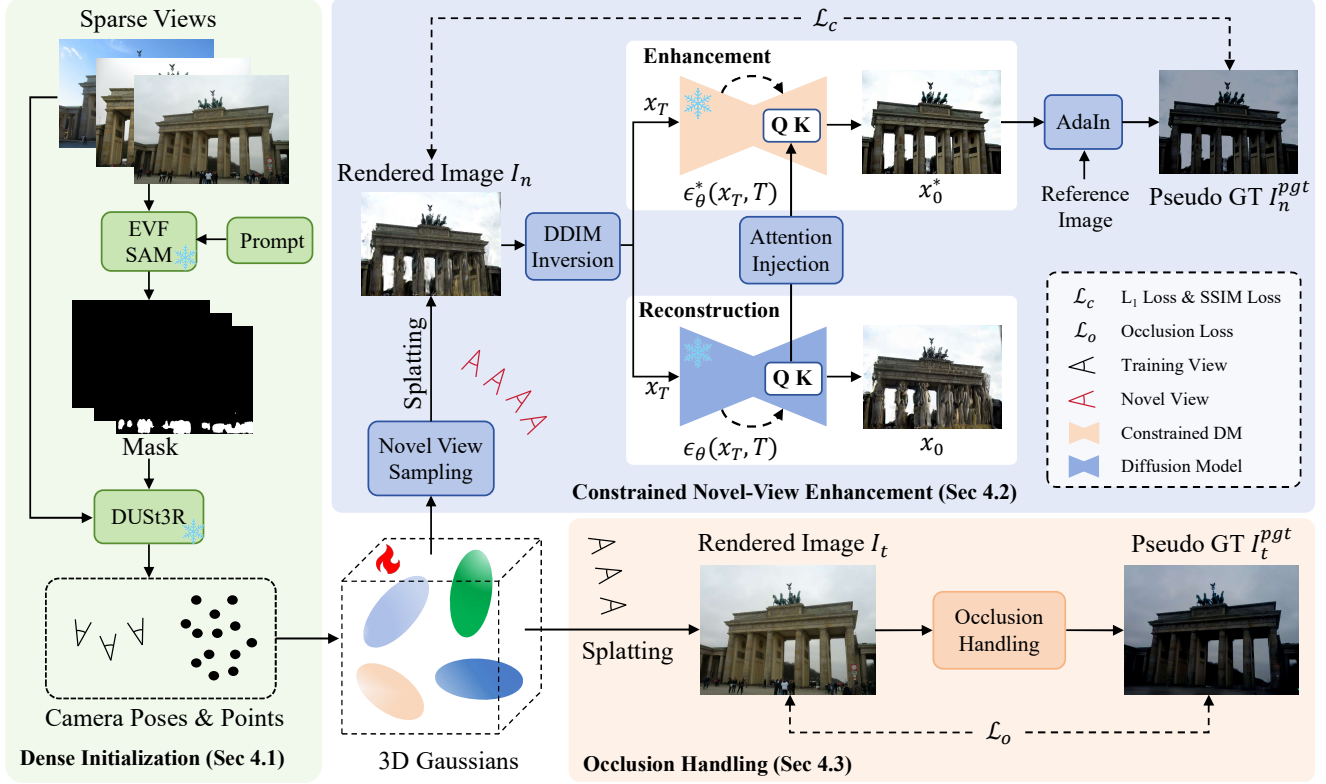


Figure 2. **An overview of the proposed SpraseGS-W framework.** Given unconstrained sparse images and user prompt, we perform dense initialization to obtain the initial point cloud, camera parameters, and occlusion masks. Then, we propose leveraging constrained diffusion priors to iteratively enhance the novel views rendered from the Gaussian radiance field and remove transient occluders.

where  $\mathbf{1}$  is a same-shape matrix as  $M_i$  but with all elements being 1,  $\mathcal{N}(\mu, \sigma^2)$  represents Gaussian noise with mean  $\mu$  and variance  $\sigma^2$  derived from non-masked regions and  $\odot$  denotes element-wise multiplication. We refine the Eq. (5) as follows:

$$P_{\mathcal{M}}, C = \mathcal{G}_\theta(\mathcal{I}_{\mathcal{M}}). \quad (7)$$

## 4.2. Constrained Novel-View Enhancement

We aim to enhance the low-quality images rendered from the Gaussian radiance field. To avoid content shift during enhancement, we use sparse training views as anchors to fine-tune the diffusion model, thus constraining the generative space to a clean subspace. To distinguish it from the original diffusion model  $\epsilon_\theta(x_t, t)$ , the constrained DM is denoted as  $\epsilon_\theta^*(x_t, t)$ .

For each rendered image  $I_n$  from a sampled novel view, we apply DDIM Inversion [35] to convert it into a standard Gaussian distribution  $x_T$ . Subsequently,  $x_T$  is input into two branches of reverse diffusion processes. The reconstruction process gradually denoises  $x_T$  to reconstruct the original rendered image using  $\epsilon_\theta(x_t, t)$ , while the enhancement process focuses on generating the high-quality image  $x_0^*$  using  $\epsilon_\theta^*(x_t, t)$ .

As shown in Fig. 3, we observe that although the con-

strained diffusion model can effectively restrict the generative space to produce high-quality novel views with the same content, it struggles to accurately preserve structure of the image, resulting in poor 3D consistency. To this end, we propose to inject structural features from the original rendered images into the enhancement process. Specifically, we use  $Q_r$  and  $K_r$  to denote the query and key from the self-attention block in the reconstruction process, while  $Q_e$ ,  $K_e$  and  $V_e$  refer to the query, key and value from the enhancement process. The attention injection operation is performed by replacing  $Q_e$  and  $K_e$  with  $Q_r$  and  $K_r$  in Eq. (4):

$$F_e = \text{softmax} \left( \frac{Q_r K_r^T}{\sqrt{d}} \right) V_e. \quad (8)$$

Here, the output feature  $F_e$  is utilized by the constrained  $\epsilon_\theta^*(x_t, t)$  to predict noise during the enhancement process. After  $T$  steps of denoising, we obtain a high-quality image  $x_0^*$  that preserves the content while eliminating artifacts.

As it is challenging to model the appearance variation from sparse images, instead of training an extraction network, we utilize AdaIn [10] to control the appearance of  $x_0^*$  based on a user-provided reference image. The resulting image serves as the pseudo ground truth  $I_n^{pgt}$  to supervise the original rendered image  $I_n$ , as defined in Eq. (13).

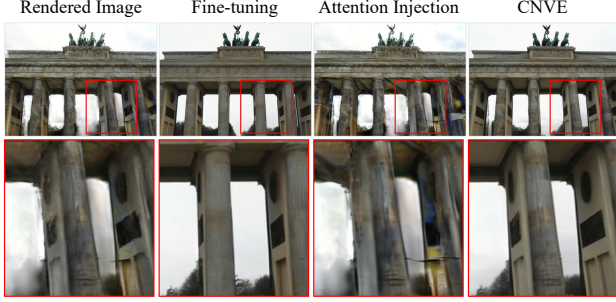


Figure 3. **Visualization results of CNVE module.** CNVE module can generate high-quality images by fine-tuning on the training views, but it struggles to preserve local image structure (the first pillar on the left in the zoom-in part). Injecting self-attention features helps maintain structure but cannot effectively remove artifacts. By combining these two strategies, CNVE achieves restoring high-fidelity, view-consistent novel views.

Through this strategy, the appearance of the reference image is seamlessly integrated into the scene, achieving appearance consistency without additional training cost.

### 4.3. Occlusion Handling

Prior works [2, 40, 44, 46, 49] utilized neural networks to optimize image-dependent 2D visibility maps from dense training images. However, these methods face significant challenges when applied in a few-shot setting. Furthermore, their unsupervised manner lacks flexibility, making it difficult to remove specific occlusions based on user preference. To address these issues, we utilize a pre-trained segmentation network EVF-SAM [52] to flexibly obtain occlusion masks  $\mathcal{M}$ , as mentioned in Sec. 4.1. Subsequently, by treating the inpainting of occlusions as a masked image enhancement task, the proposed CNVE paradigm can naturally be applied to remove occlusions in the generation space. Specifically, given a rendered image  $I_t$  from a training view and its ground truth  $I_t^{gt}$ , we use DDIM Inversion to obtain the corresponding latents  $x_T'$  and  $x_T^{gt}$ . The fused initial latent  $x_T^*$  is computed via mask  $M_i$ :

$$x_T^* = M_i \odot x_T' + (1 - M_i) \odot x_T^{gt}. \quad (9)$$

Next, similar to the process outlined in Sec. 4.2, we perform two branches of reverse diffusion processes for  $x_T^*$ . To distinguish symbols, we use a superscript to differentiate  $Q_e', K_e', V_e', Q_r', K_r'$  from  $Q_e, K_e, V_e, Q_r$  and  $K_r$ . The attention injection process is formulated as follows:

$$\begin{aligned} Q_{OH} &= M_i \odot Q_e' + (1 - M_i) \odot Q_r', \\ K_{OH} &= M_i \odot K_e' + (1 - M_i) \odot K_r', \\ F_e' &= \text{softmax} \left( \frac{Q_{OH}(K_{OH})^T}{\sqrt{d}} \right) V_e'. \end{aligned} \quad (10)$$

After  $T$  steps of denoising followed by AdaIn, we obtain a high-fidelity and occlusion-free image that serves

as pseudo ground truth  $I_t^{pgt}$ . The weighted fusion and injection operations help minimize inherent information loss during the diffusion process, ensuring the constrained SD focuses on the masked regions.

### 4.4. Progressive Sampling and Training Strategy

**Novel View Sampling.** To prevent overfitting to sparse training views, we employ novel view augmentation:

$$\begin{aligned} \mathcal{C}' &= \bigcup_{1 \leq i < j \leq N} \text{SLERP}(\mathcal{C}_i, \mathcal{C}_j, \alpha), \quad \alpha \sim \mathcal{U}(0, 1), \\ \mathcal{P}' &= \bigcup_{\mathcal{C}_k \in \mathcal{C}} (t_k + \epsilon, \mathbf{q}), \quad \epsilon \sim \mathcal{N}(\mathbf{0}, \delta), \\ \mathcal{C}^* &= \mathcal{C}' \cup \mathcal{P}'. \end{aligned} \quad (11)$$

Here, SLERP means spherical linear interpolation. The  $\mathcal{P}'$  is inspired by previous work [53].  $t_k \in \mathcal{C}_k$  denotes camera locations,  $\mathbf{q}$  is a quaternion representing the rotation averaged from the two closest training views.

**Progressive Sampling and Training.** We adapt a progressive training strategy that transitions from simple to complex views. The process begins by randomly selecting training views to optimize the Gaussians for  $\tau_c$  iterations. Subsequently, we gradually integrate sampled novel views  $\mathcal{C}^*$  into training process in three stages based on their complexity. These novel views are categorized into three levels: simple, medium, and difficult based on their Euclidean distance from the training views. To balance the trade-off between errors and useful priors introduced by the diffusion model, we sample  $\mathcal{C}^*$  for training with a probability  $\beta$ . The PSTS ultimately results in a multi-view consistent Gaussian radiance field. For further details, please refer to the supplementary material.

### 4.5. Optimization

Following 3DGS [15], we use the L1 loss  $\mathcal{L}_1$  and SSIM loss [41]  $\mathcal{L}_{SSIM}$  to measure the difference between the rendered image and the ground truth (GT) image  $I_i^{gt}$ . For the rendered training view  $I_t$ , when the iteration is less than  $\tau_o$ , we use the corresponding mask  $M_i$  to mask out transient occlusions. Once the iteration exceeds  $\tau_o$ , we employ its pseudo GT  $I_t^{pgt}$  to supervise the entire image. Let  $\overline{M}_i = 1 - M_i$ . The loss function can be written as Eq. (12). For the rendered novel view  $I_n$ , we use its pseudo GT  $I_n^{pgt}$  as the supervision mentioned in Eq. (13). The total loss function is formulated as in Eq. (14), where  $\lambda_1$ ,  $\lambda_2$  and  $\lambda_3$  are 0.8, 0.2, 1.0, respectively.

$$\mathcal{L}_o = \begin{cases} \mathcal{L}_c(\overline{M}_i \odot I_t, \overline{M}_i \odot I_i^{gt}), & \text{if iteration} < \tau_o; \\ \mathcal{L}_c(I_t, I_t^{pgt}), & \text{if iteration} \geq \tau_o. \end{cases} \quad (12)$$

$$\mathcal{L}_c(I_n, I_n^{pgt}) = \lambda_1 \mathcal{L}_1(I_n, I_n^{pgt}) + \lambda_2 \mathcal{L}_{SSIM}(I_n, I_n^{pgt}). \quad (13)$$

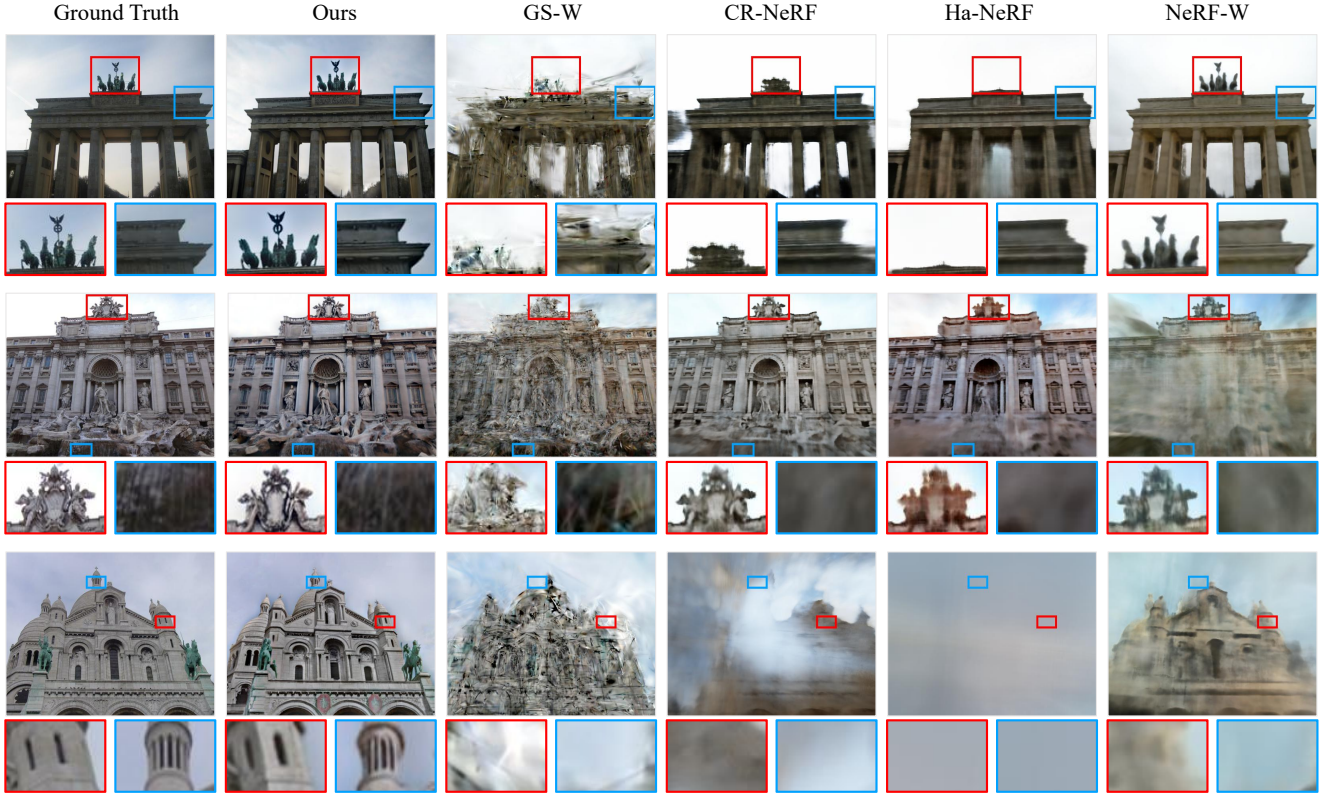


Figure 4. **Qualitative Comparison on PhotoTourism dataset.** Under the condition of sparse views, SparseGS-W is able to reconstruct more realistic and detailed scenes with less artifacts and blurring.

Method	PSNR $\uparrow$	SSIM $\uparrow$	LPIPS $\downarrow$	FID $\downarrow$	MUSIQ $\uparrow$	ClipIQA $\uparrow$	TT(m)	FPS
NeRF-W [22]	14.20	0.54	0.51	206	33.15	0.27	60	<0.1
Ha-NeRF [2]	11.73	0.48	0.38	164	27.71	0.19	58	<0.1
CR-NeRF [46]	15.08	0.59	0.47	202	36.72	0.23	39	<0.1
3DGS [15]/3DGS $\dagger$	13.61/13.99	0.45/0.40	0.49/0.48	201/134	55.01/60.51	0.33/0.35	8/9	191
GS-W [49]/GS-W $\dagger$	14.02/14.80	0.48/0.50	0.46/0.49	257/159	58.11/47.32	0.32/0.27	50/70	81
WildGS [17]/WildGS $\dagger$	11.78/14.73	0.39/0.41	0.51/0.46	269/119	47.55/ 60.70	0.33/ 0.36	420/603	117*
<b>SparseGS-W<math>\dagger</math>(Ours)</b>	<b>19.01</b>	<b>0.55</b>	<b>0.31</b>	<b>48</b>	<b>66.98</b>	<b>0.51</b>	<b>118</b>	<b>112</b>

Table 1. **Quantitative Comparison on PhotoTourism dataset for 5 input views.** We color each cell as **best** and **second best**.  $\dagger$  denotes using the same initial point cloud and camera poses from DUST3R for fair comparisons, otherwise using sparse points and poses from COLMAP. WildGaussians is abbreviated as WildGS for brevity. \* means number from the paper. TT denotes training time.

$$\mathcal{L} = \mathcal{L}_o + \lambda_3 \mathcal{L}_c. \quad (14)$$

## 5. Experiments

### 5.1. Experimental Setup

**Dataset.** Since the few-shot novel view synthesis on large-scale **PhotoTourism datasets** [12] is a novel and more challenging task, we do not utilize the exact same test set as previous methods based on dense training views. For each scene, we select 10 images from various view-points as the test set and select 5 images as the training set for all methods. Notably, we not only follow previous works [2, 46, 49] by using the same three scenes: Branden-

burg Gate, Sacre Coeur, and Trevi Fountain, but also include additional scenes: Palace of Westminster and Pantheon Exterior. To further validate the robustness of our method, we compare it with several sparse-view methods on the **Tanks and Temples dataset**. For each scene, we sample 3 views from every 8-frame clip as the training set and test on the remaining 1/8 of the images at a resolution of  $688 \times 512$ .

**Metrics and baselines.** We report quantitative results of the full-reference metrics PSNR, SSIM [41], and LPIPS [51]. We observe that the results of SSIM do not align with the visual quality of the image, a phenomenon also mentioned in the field of image restora-

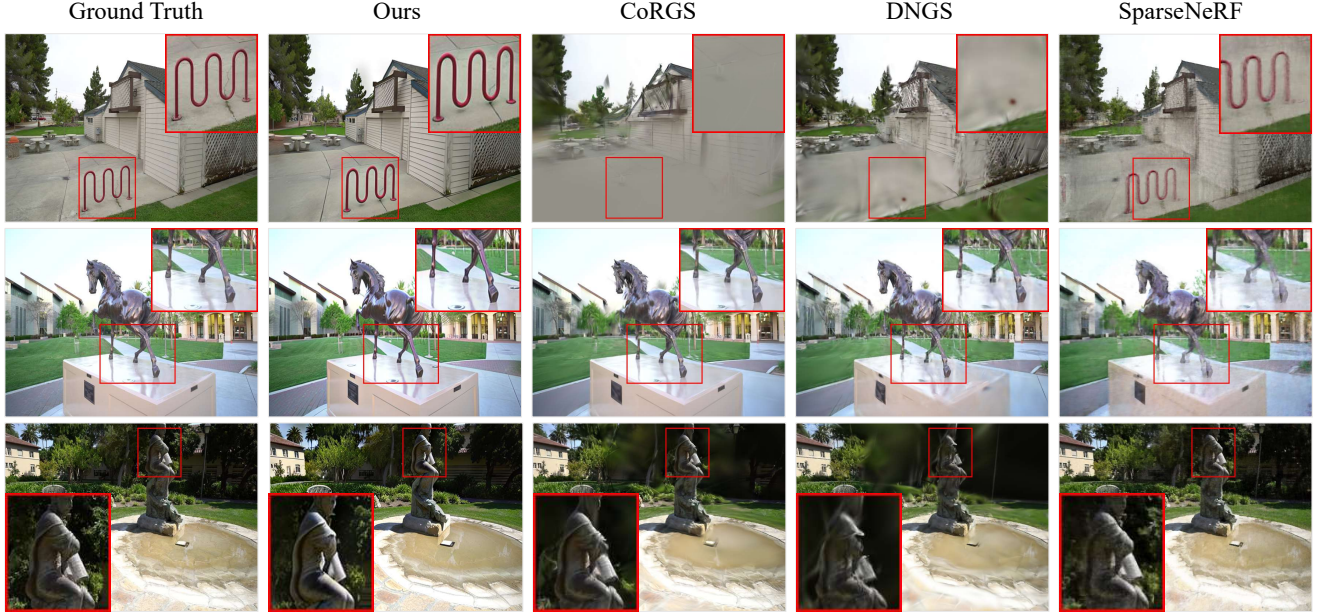


Figure 5. **Qualitative Comparison on Tanks and Temples dataset.** Our method outperforms other baselines in the task of few-shot NVS.

Method	PSNR $\uparrow$	SSIM $\uparrow$	LPIPS $\downarrow$	FID $\downarrow$	MUSIQ $\uparrow$	ClipIQA $\uparrow$	TT(m)	FPS
SparseNeRF [37]	19.13	0.55	0.44	191	44.66	0.25	73	<0.1
3DGS [15]/3DGS $\dagger$	16.01/16.99	0.43/0.55	0.42/0.36	182/200	64.03/63.59	0.38/0.41	5/7	317/291
FSGS [53]/FSGS $\dagger$	17.17/18.11	0.53/0.52	0.42/0.34	205/126	59.24/62.51	0.28/0.33	20/21	297/170
DNGS [18]/DNGS $\dagger$	18.32/19.30	0.56/0.56	0.43/0.32	216/105	57.46/66.13	0.30/ 0.46	7/8	286/79
CoRGS [50]/CoRGS $\dagger$	19.03/ 19.92	0.59/ 0.63	0.37/ 0.27	269/ 72	65.05/ 68.11	0.29/0.41	7/14	238/149
<b>Sparse-GS<math>\dagger</math>(Ours)</b>	<b>21.58</b>	<b>0.68</b>	<b>0.22</b>	<b>55</b>	<b>69.80</b>	<b>0.50</b>	<b>28</b>	<b>102</b>

Table 2. **Quantitative Comparison on Tanks and Temples dataset for 3 input views.** We color each cell as **best** and **second best**.  $\dagger$  denotes using the same initial point cloud and camera poses from DUST3R for fair comparisons, otherwise using sparse points and poses from COLMAP. TT represents the training time, measured in minutes.

tion [1, 7, 13, 48]. Therefore, to provide a more comprehensive evaluation, we also report the non-reference metrics FID [8], ClipIQA [38], and MUSIQ [14] for all methods. We evaluate our method against the SOTA open-source in-the-wild methods NeRF-W [22], Ha-NeRF [2], CR-NeRF [46], 3DGS [15], GS-W [49], and WildGaussians [17]. Additionally, we include comparisons with several SOTA few-shot methods SparseNeRF [37], FSGS [53], DNGS [19], and CoRGS [50].

**Implementation Details.** We implement our method using PyTorch [28]. To constrain the generative space, we fine-tune Stable Diffusion V1.5 using DreamBooth [33] for 400 iterations with a batch size of 1 and a learning rate of  $2 \times 10^{-6}$ , which takes less than 2 minutes. For PhotoTourism datasets, we use the **prompt “tourist”** to generate masks  $\mathcal{M}$  predicted by EVF-SAM [52] and train our model on a single NVIDIA RTX 4090 GPU for a total of 7,500 iterations. Specifically, to ensure stability, we first train on the training views for  $\tau_c = 5,500$  iteration, followed by 2,000 iterations applying the CNVE module with  $\beta$  set to

0.3. The OH module is applied at the  $\tau_o = 6,500$  iteration. For Tanks and Temples dataset, we train the model with 1,000 iterations and the CNVE module is applied after 500 iterations. The OH module is not utilized in this case, as there are no occlusions present in this dataset. We follow other hyperparameter settings as 3DGS [15], except without using adaptive density control. We set the DDIM sampling and inversion steps  $T$  to 50.

## 5.2. Comparison

**PhotoTourism.** Quantitative results and visualizations are shown in Tab. 1 and Fig. 4. Our method demonstrates significant performance improvements over state-of-the-art methods. Compared to the representative NeRF-based method CR-NeRF [46], our method achieves notable enhancements, with PSNR, LPIPS, and FID improved by +25.7%, +34.0% and +76.2%, respectively. Compared to the representative 3DGS-based methods GS-W [49] with the same initial points and camera poses, our method improves the PSNR, LPIPS and FID by +28.1%, +36.7% and

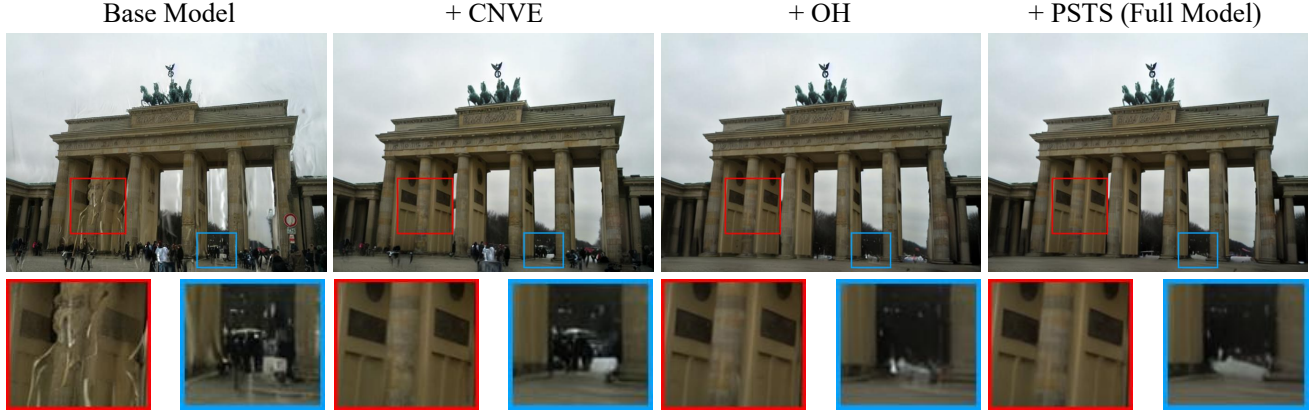


Figure 6. **Qualitative results of ablation studies.** With the proposed CNVE, OH modules and the PSTS, SparseGS-W effectively eliminates transient occlusions and removes numerous artifacts, significantly enhancing the results in the few-shot scenarios.

	PSNR $\uparrow$	SSIM $\uparrow$	LPIPS $\downarrow$	FID $\downarrow$	MUSIQ $\uparrow$	ClipIQA $\uparrow$
Base Model	15.38	0.48	0.43	116	59.99	0.31
+ CNVE	18.42	0.52	0.36	110	62.63	0.46
+ OH	18.70	0.54	0.32	48	66.84	0.47
+ PSTS (Full)	19.01	0.55	0.31	48	66.98	0.51

Table 3. **Ablation study on PhotoTourism dataset.**

+69.8%, respectively. In particular, comparisons with GS-W and WildGaussians under the same point cloud and camera parameters demonstrate the effectiveness of our framework. Our method provides additional multi-view supervision, which guides the optimization of Gaussians and represents illumination changes.

**Tanks and Temples.** To evaluate the robustness of our framework, we conduct experiments on the Tanks and Temples dataset, which does not contain dynamic appearance changes and transient occlusions. Quantitative results and visualizations are presented in Tab. 2 and Fig. 5. Our method not only achieves the highest scores across all full-reference and non-reference metrics but also demonstrates superior visual quality. These results show that the framework we designed for sparse large-scale Internet photo collections has robustness to expand to more general scenarios.

### 5.3. Ablation studies

In Tab. 3 and Fig. 6, we ablate our method on PhotoTourism 5-view setting. Base Model extends 3DGS by integrating DUS3R. From the zoomed-in details in the red box, we observe that the *Constrained Novel-View Enhancement* (CNVE) module significantly reduces artifacts, improves rendering quality, and reshapes scene geometry. After adding the *Occlusion Handling* (OH) module, pedestrians are effectively removed from the scene. The zoomed-in details in the blue box demonstrate the effectiveness of the *Progressive Sampling and Training Strategy* (PSTS) in improving high-frequency details within the scene.

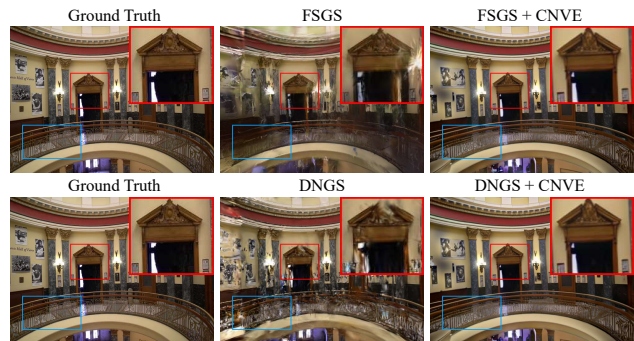


Figure 7. **Visualization Results of plug-and-play CNVE.**

Method	PSNR $\uparrow$	SSIM $\uparrow$	LPIPS $\downarrow$	FID $\downarrow$	MUSIQ $\uparrow$	ClipIQA $\uparrow$	TT(m)
FSGS [53]	17.17	0.53	0.42	205	59.24	0.28	20
FSGS+CNVE	19.28	0.57	0.34	114	68.01	0.51	60
DNGS [18]	18.32	0.56	0.43	216	57.46	0.30	7
DNGS+CNVE	19.01	0.54	0.40	132	60.73	0.39	39

Table 4. **Quantitative results of plug-and-play CNVE.**

### 5.4. Plug-and-play CNVE experiment

We validate our plug-and-play CNVE module on Tanks and Temples under the 3-view setting. Visualization and quantitative results are reported in Fig. 7 and Tab. 4. The results show that the CNVE module effectively improves the rendering quality and recovers complete geometric structures with only a modest increase in training time.

## 6. Conclusion

In this paper, we propose SparseGS-W, a novel framework for reconstructing unconstrained in-the-wild scenes with as few as five training images by leveraging constrained diffusion priors. We believe that our method is a step forward towards real-world applications. However, estimating the camera poses in the sparse-view setting is a challenging problem. Our method struggles with poor initial camera poses. We leave it for future work.



## References

- [1] Yochai Blau and Tomer Michaeli. The perception-distortion tradeoff. In *Proceedings of the IEEE Conference on Computer Vision and Pattern Recognition*, pages 6228–6237, 2018. 7
- [2] Xingyu Chen, Qi Zhang, Xiaoyu Li, Yue Chen, Ying Feng, Xuan Wang, and Jue Wang. Hallucinated neural radiance fields in the wild. In *Proceedings of the IEEE/CVF Conference on Computer Vision and Pattern Recognition*, pages 12943–12952, 2022. 2, 5, 6, 7
- [3] Hiba Dahmani, Moussab Bennehar, Nathan Piasco, Luis Roldao, and Dzmitry Tsishkou. Swag: Splatting in the wild images with appearance-conditioned gaussians. *arXiv preprint arXiv:2403.10427*, 2024. 2
- [4] Kangle Deng, Andrew Liu, Jun-Yan Zhu, and Deva Ramanan. Depth-supervised nerf: Fewer views and faster training for free. In *Proceedings of the IEEE/CVF Conference on Computer Vision and Pattern Recognition*, pages 12882–12891, 2022. 2
- [5] Prafulla Dhariwal and Alexander Nichol. Diffusion models beat gans on image synthesis. *Advances in Neural Information Processing Systems*, 34:8780–8794, 2021. 3
- [6] Ruiqi Gao, Aleksander Holynski, Philipp Henzler, Arthur Brussee, Ricardo Martin-Brualla, Pratul Srinivasan, Jonathan T Barron, and Ben Poole. Cat3d: Create anything in 3d with multi-view diffusion models. *arXiv preprint arXiv:2405.10314*, 2024. 3
- [7] Jinjin Gu, Haoming Cai, Chao Dong, Jimmy S Ren, Radu Timofte, Yuan Gong, Shanshan Lao, Shuwei Shi, Jiahao Wang, Sidi Yang, et al. Ntire 2022 challenge on perceptual image quality assessment. In *Proceedings of the IEEE/CVF Conference on Computer Vision and Pattern Recognition*, pages 951–967, 2022. 7
- [8] Martin Heusel, Hubert Ramsauer, Thomas Unterthiner, Bernhard Nessler, and Sepp Hochreiter. Gans trained by a two time-scale update rule converge to a local nash equilibrium. *Advances in Neural Information Processing Systems*, 30, 2017. 7
- [9] Jonathan Ho, Ajay Jain, and Pieter Abbeel. Denoising diffusion probabilistic models. *Advances in Neural Information Processing Systems*, 33:6840–6851, 2020. 3
- [10] Xun Huang and Serge Belongie. Arbitrary style transfer in real-time with adaptive instance normalization. In *Proceedings of the IEEE International Conference on Computer Vision*, pages 1501–1510, 2017. 2, 4
- [11] Ajay Jain, Matthew Tancik, and Pieter Abbeel. Putting nerf on a diet: Semantically consistent few-shot view synthesis. In *Proceedings of the IEEE/CVF International Conference on Computer Vision*, pages 5885–5894, 2021. 2
- [12] Yuhe Jin, Dmytro Mishkin, Anastasiia Mishchuk, Jiri Matas, Pascal Fua, Kwang Moo Yi, and Eduard Trulls. Image matching across wide baselines: From paper to practice. *International Journal of Computer Vision*, 129(2):517–547, 2021. 6
- [13] Gu Jinjin, Cai Haoming, Chen Haoyu, Ye Xiaoxing, Jimmy S Ren, and Dong Chao. Pipal: a large-scale image quality assessment dataset for perceptual image restoration. In *Computer Vision—ECCV 2020: 16th European Conference, Glasgow, UK, August 23–28, 2020, Proceedings, Part XI 16*, pages 633–651, 2020. 7
- [14] Junjie Ke, Qifei Wang, Yilin Wang, Peyman Milanfar, and Feng Yang. Musiq: Multi-scale image quality transformer. In *Proceedings of the IEEE/CVF International Conference on Computer Vision*, pages 5148–5157, 2021. 7
- [15] Bernhard Kerbl, Georgios Kopanas, Thomas Leimkühler, and George Drettakis. 3d gaussian splatting for real-time radiance field rendering. *ACM Transactions on Graphics(ToG)*, 42(4):139–1, 2023. 1, 2, 3, 5, 6, 7
- [16] Mijeong Kim, Seonguk Seo, and Bohyung Han. Infonerf: Ray entropy minimization for few-shot neural volume rendering. In *Proceedings of the IEEE/CVF Conference on Computer Vision and Pattern Recognition*, pages 12912–12921, 2022. 2
- [17] Jonas Kulhanek, Songyou Peng, Zuzana Kukelova, Marc Pollefeys, and Torsten Sattler. Wildgaussians: 3d gaussian splatting in the wild. *Advances in Neural Information Processing Systems*, 2024. 1, 2, 6, 7
- [18] Jiahe Li, Jiawei Zhang, Xiao Bai, Jin Zheng, Xin Ning, Jun Zhou, and Lin Gu. Dngaussian: Optimizing sparse-view 3d gaussian radiance fields with global-local depth normalization. In *Proceedings of the IEEE/CVF Conference on Computer Vision and Pattern Recognition*, pages 20775–20785, 2024. 7, 8
- [19] Jiahe Li, Jiawei Zhang, Xiao Bai, Jin Zheng, Xin Ning, Jun Zhou, and Lin Gu. Dngaussian: Optimizing sparse-view 3d gaussian radiance fields with global-local depth normalization. In *Proceedings of the IEEE/CVF Conference on Computer Vision and Pattern Recognition*, pages 20775–20785, 2024. 2, 7
- [20] Ruoshi Liu, Rundi Wu, Basile Van Hoorick, Pavel Tokmakov, Sergey Zakharov, and Carl Vondrick. Zero-1-to-3: Zero-shot one image to 3d object. In *Proceedings of the IEEE/CVF International Conference on Computer Vision*, pages 9298–9309, 2023. 3
- [21] Xi Liu, Chaoyi Zhou, and Siyu Huang. 3dgs-enhancer: Enhancing unbounded 3d gaussian splatting with view-consistent 2d diffusion priors. *Advances in Neural Information Processing Systems*, 2024. 2, 3
- [22] Ricardo Martin-Brualla, Noha Radwan, Mehdi SM Sajjadi, Jonathan T Barron, Alexey Dosovitskiy, and Daniel Duckworth. Nerf in the wild: Neural radiance fields for unconstrained photo collections. In *Proceedings of the IEEE/CVF Conference on Computer Vision and Pattern Recognition*, pages 7210–7219, 2021. 2, 6, 7
- [23] Ben Mildenhall, Pratul P Srinivasan, Matthew Tancik, Jonathan T Barron, Ravi Ramamoorthi, and Ren Ng. Nerf: Representing scenes as neural radiance fields for view synthesis. *Communications of the ACM*, 65(1):99–106, 2021. 1, 2
- [24] Chong Mou, Xintao Wang, Jiechong Song, Ying Shan, and Jian Zhang. Diffeditor: Boosting accuracy and flexibility on diffusion-based image editing. In *Proceedings of the IEEE/CVF Conference on Computer Vision and Pattern Recognition*, pages 8488–8497, 2024. 3

- [25] Michael Niemeyer, Jonathan T Barron, Ben Mildenhall, Mehdi SM Sajjadi, Andreas Geiger, and Noha Radwan. Regnerf: Regularizing neural radiance fields for view synthesis from sparse inputs. In *Proceedings of the IEEE/CVF Conference on Computer Vision and Pattern Recognition*, pages 5480–5490, 2022. 2
- [26] Maxime Oquab, Timothée Darcet, Théo Moutakanni, Huy Vo, Marc Szafraniec, Vasil Khalidov, Pierre Fernandez, Daniel Haziza, Francisco Massa, Alaaeldin El-Nouby, et al. Dinov2: Learning robust visual features without supervision. *Transactions on Machine Learning Research Journal*, pages 1–31, 2024. 2
- [27] Avinash Paliwal, Wei Ye, Jinhui Xiong, Dmytro Kotovenko, Rakesh Ranjan, Vikas Chandra, and Nima Khademi Kalantari. Coherentgts: Sparse novel view synthesis with coherent 3d gaussians. In *European Conference on Computer Vision*, 2024. 2
- [28] Adam Paszke, Sam Gross, Francisco Massa, Adam Lerer, James Bradbury, Gregory Chanan, Trevor Killeen, Zeming Lin, Natalia Gimelshein, Luca Antiga, et al. Pytorch: An imperative style, high-performance deep learning library. *Advances in Neural Information Processing Systems*, 32, 2019. 7
- [29] Ben Poole, Ajay Jain, Jonathan T Barron, and Ben Mildenhall. Dreamfusion: Text-to-3d using 2d diffusion. In *The Eleventh International Conference on Learning Representations*, 2023. 3
- [30] Guocheng Qian, Jinjie Mai, Abdullah Hamdi, Jian Ren, Aliaksandr Siarohin, Bing Li, Hsin-Ying Lee, Ivan Skokhodov, Peter Wonka, Sergey Tulyakov, et al. Magic123: One image to high-quality 3d object generation using both 2d and 3d diffusion priors. In *ICLR*, 2024. 3
- [31] Barbara Roessle, Jonathan T Barron, Ben Mildenhall, Pratul P Srinivasan, and Matthias Nießner. Dense depth priors for neural radiance fields from sparse input views. In *Proceedings of the IEEE/CVF Conference on Computer Vision and Pattern Recognition*, pages 12892–12901, 2022. 2
- [32] Robin Rombach, Andreas Blattmann, Dominik Lorenz, Patrick Esser, and Björn Ommer. High-resolution image synthesis with latent diffusion models. In *Proceedings of the IEEE/CVF Conference on Computer Vision and Pattern Recognition*, pages 10684–10695, 2022. 3
- [33] Nataniel Ruiz, Yuanzhen Li, Varun Jampani, Yael Pritch, Michael Rubinstein, and Kfir Aberman. Dreambooth: Fine tuning text-to-image diffusion models for subject-driven generation. In *Proceedings of the IEEE/CVF Conference on Computer Vision and Pattern Recognition*, pages 22500–22510, 2023. 7
- [34] Seunghyeon Seo, Yeonjin Chang, and Nojun Kwak. Flipnerf: Flipped reflection rays for few-shot novel view synthesis. In *Proceedings of the IEEE/CVF International Conference on Computer Vision*, pages 22883–22893, 2023. 2
- [35] Jiaming Song, Chenlin Meng, and Stefano Ermon. Denoising diffusion implicit models. In *International Conference on Learning Representations*, 2020. 4
- [36] Narek Tumanyan, Michal Geyer, Shai Bagon, and Tali Dekel. Plug-and-play diffusion features for text-driven image-to-image translation. In *Proceedings of the IEEE/CVF Conference on Computer Vision and Pattern Recognition*, pages 1921–1930, 2023. 3
- [37] Guangcong Wang, Zhaoxi Chen, Chen Change Loy, and Ziwei Liu. Sparsenerf: Distilling depth ranking for few-shot novel view synthesis. In *Proceedings of the IEEE/CVF International Conference on Computer Vision*, pages 9065–9076, 2023. 2, 7
- [38] Jianyi Wang, Kelvin CK Chan, and Chen Change Loy. Exploring clip for assessing the look and feel of images. In *Proceedings of the AAAI Conference on Artificial Intelligence*, pages 2555–2563, 2023. 7
- [39] Shuzhe Wang, Vincent Leroy, Yohann Cabon, Boris Chidlovskii, and Jerome Revaud. Dust3r: Geometric 3d vision made easy. In *Proceedings of the IEEE/CVF Conference on Computer Vision and Pattern Recognition*, pages 20697–20709, 2024. 3
- [40] Yuze Wang, Junyi Wang, and Yue Qi. We-gs: An in-the-wild efficient 3d gaussian representation for unconstrained photo collections. *arXiv preprint arXiv:2406.02407*, 2024. 2, 5
- [41] Zhou Wang, Alan C Bovik, Hamid R Sheikh, and Eero P Simoncelli. Image quality assessment: from error visibility to structural similarity. *IEEE transactions on image processing*, 13(4):600–612, 2004. 5, 6
- [42] Zhengyi Wang, Cheng Lu, Yikai Wang, Fan Bao, Chongxuan Li, Hang Su, and Jun Zhu. Prolificdreamer: High-fidelity and diverse text-to-3d generation with variational score distillation. *Advances in Neural Information Processing Systems*, 36, 2024. 3
- [43] Jamie Wynn and Daniyar Turmukhambetov. Diffusionerf: Regularizing neural radiance fields with denoising diffusion models. In *Proceedings of the IEEE/CVF Conference on Computer Vision and Pattern Recognition*, pages 4180–4189, 2023. 2
- [44] Jiacong Xu, Yiqun Mei, and Vishal M Patel. Wild-gs: Real-time novel view synthesis from unconstrained photo collections. *Advances in Neural Information Processing Systems*, 2024. 2, 5
- [45] Jiawei Yang, Marco Pavone, and Yue Wang. Freenerf: Improving few-shot neural rendering with free frequency regularization. In *Proceedings of the IEEE/CVF Conference on Computer Vision and Pattern Recognition*, pages 8254–8263, 2023. 2
- [46] Yifan Yang, Shuhai Zhang, Zixiong Huang, Yubing Zhang, and Mingkui Tan. Cross-ray neural radiance fields for novel-view synthesis from unconstrained image collections. In *Proceedings of the IEEE/CVF International Conference on Computer Vision*, pages 15901–15911, 2023. 2, 5, 6, 7
- [47] Alex Yu, Vickie Ye, Matthew Tancik, and Angjoo Kanazawa. pixelnerf: Neural radiance fields from one or few images. In *Proceedings of the IEEE/CVF Conference on Computer Vision and Pattern Recognition*, pages 4578–4587, 2021. 2
- [48] Fanghua Yu, Jinjin Gu, Zheyuan Li, Jinfan Hu, Xiangtao Kong, Xintao Wang, Jingwen He, Yu Qiao, and Chao Dong. Scaling up to excellence: Practicing model scaling for photo-realistic image restoration in the wild. In *Proceedings of the IEEE/CVF Conference on Computer Vision and Pattern Recognition*, pages 25669–25680, 2024. 7

- [49] Dongbin Zhang, Chuming Wang, Weitao Wang, Peihao Li, Minghan Qin, and Haoqian Wang. Gaussian in the wild: 3d gaussian splatting for unconstrained image collections. In *European Conference on Computer Vision*, 2024. [1](#), [2](#), [5](#), [6](#), [7](#)
- [50] Jiawei Zhang, Jiahe Li, Xiaohan Yu, Lei Huang, Lin Gu, Jin Zheng, and Xiao Bai. Cor-gs: sparse-view 3d gaussian splatting via co-regularization. In *European Conference on Computer Vision*, pages 335–352, 2025. [2](#), [7](#)
- [51] Richard Zhang, Phillip Isola, Alexei A Efros, Eli Shechtman, and Oliver Wang. The unreasonable effectiveness of deep features as a perceptual metric. In *Proceedings of the IEEE Conference on Computer Vision and Pattern Recognition*, pages 586–595, 2018. [6](#)
- [52] Yuxuan Zhang, Tianheng Cheng, Rui Hu, Heng Liu, Longjin Ran, Xiaoxin Chen, Wenyu Liu, Xinggang Wang, et al. Evfsam: Early vision-language fusion for text-prompted segment anything model. *arXiv preprint arXiv:2406.20076*, 2024. [3](#), [5](#), [7](#)
- [53] Zehao Zhu, Zhiwen Fan, Yifan Jiang, and Zhangyang Wang. Fsgs: Real-time few-shot view synthesis using gaussian splatting. In *European Conference on Computer Vision*, pages 145–163, 2025. [2](#), [5](#), [7](#), [8](#)